Tungsten Oxytetrachloride as a Positive Electrode for Chloride-Ion Batteries

Guruprakash Karkera,* Mervyn Soans, Bosubabu Dasari, Ediga Umeshbabu, Musa Ali Cambaz, Zhen Meng, Thomas Diemant, and Maximilian Fichtner*

Rechargeable chloride-ion batteries (CIBs) are a new emerging battery technology that can potentially provide high theoretical volumetric capacities at lower cost and higher abundance. However, research on CIBs is in its early stages, and the current challenge lies in finding suitable electrodes and electrolytes. Herein, tungsten oxychloride is introduced for the first time as a cathode candidate for use in CIB. $WOCl_4$ enables the reversible transfer of nearly one Cl^- per formula unit during electrochemical cycling, corresponding to an initial discharge capacity of 120 mAh g^{-1}. A reversible capacity of 90 mAh g^{-1} (75%) is retained after 50 cycles. Postmortem analysis of cycled electrodes by X-ray diffraction, X-ray photoelectron spectroscopy, and Raman spectroscopy reveals the reversible chloride-ion transfer between the electrodes through a conversion mechanism. This work paves the way for the use of tungsten chloride-based electrode materials for battery applications.

1. Introduction

Lithium-ion batteries (LIB) have played a predominant role in the portable electronics space for over two decades and recently they have also seen growing demands to meet more challenging applications such as long-range electric vehicles, stationary, and mobile applications.[1] However, due to the increasing depletion of lithium resources around the world, it is essential to explore other suitable electroactive species, which can be economically extracted from cheap, naturally abundant raw materials to establish a sustainable and economically viable value chain in the field of energy storage.[2] Recently, much emphasis has been placed on chemistries operating on the cationic shuttle of Na^+, K^+, Mg^{2+}, Ca^{2+}, and Zn^{2+} ions and anionic shuttle based on F^- and Cl^- ion.[3] One promising alternative to LIBs is rechargeable chloride-ion batteries (CIBs)[4] which offer high theoretical volumetric energy densities up to 2500 Wh L^{-1}, comparable with lithium–sulfur batteries.[5] Energy storage based on chloride-ion transfer would be favorable due to the lower cost and higher abundance of chlorides as compared with lithium.[6] The first proof of concept of a CIB was demonstrated by Zhao et al., with $CoCl_2$, VCl_3, and $BiCl_3$ cathodes, which suffered from rapid capacity fading during cycling attributed to the high volume changes due to the underlying conversion-based storage mechanism and solubility issues of cathodes in the electrolyte.[7] Layered double hydroxides, which are less prone to dissolve in the electrolyte, could demonstrate a cyclability of CIBs beyond 1000 cycles.[8] Recently, chloride-ion-intercalated graphite was used as a cathode in combination with aqueous electrolytes and demonstrated the feasibility of a high cycle life with over 4000 cycles.[9] Furthermore, progress has also been shown in the development of inorganic chloride-ion-conducting solid electrolyte $CsSnCl_3$ with a large electrochemical stability window of 6.1 V and a room temperature conductivity of $\approx10^{-4}$ S cm^{-1}.[5d,10]

In general, the field of CIB holds great promise for the exploration of novel electrode materials. Mixed-anion transition metal-based oxychloride materials are potential candidates for electrodes, that can offer better structural stability and facilitate solvent processing as compared with their chloride analogues. The layered VOCl cathode investigated by Gao et al. demonstrated stable cycling performance with a reversible capacity of 113 mAh g^{-1} after 100 cycles.[5a] Other examples like FeOCl[11] and BiOCl[3g] could be used as cathode material for CIBs and exhibited moderate electrochemical performances. Both VOCl and FeOCl have an orthorhombic structure, with a layered arrangement of chloride and oxygen atoms, while Fe^{3+}/V^{3+} is incorporated at the center of the polyhedron. In contrast, BiOCl has a tetragonal structure, where chloride ions lie between the Bi and O bilayers. In this report, we evaluate the electrochemical performance of tetragonal-structured tungsten oxytetrachloride ($WOCl_4$) as an electrode material for CIBs (theoretical

G. Karkera, M. Soans, E. Umeshbabu, M. A. Cambaz, Z. Meng,
T. Diemant, M. Fichtner
Helmholtz Institute Ulm (HIU) for Electrochemical Energy Storage
89081 Ulm, Germany
E-mail: karkera.guruprakash@uni-ulm.de

B. Dasari, M. Fichtner
Institute of Nanotechnology (INT)
Karlsruhe Institute of Technology (KIT)
76344 Eggenstein-Leopoldshafen, 76344 Karlsruhe, Germany
E-mail: m.fichtner@kit.edu

The ORCID identification number(s) for the author(s) of this article can be found under https://doi.org/10.1002/ente.202200193.

capacity of 313 mAh g^{-1}). To the best of our knowledge, this is the first report of $WOCl_4$ as a cathode material for CIB. The phase purity of $WOCl_4$ was demonstrated by a combination of diffraction and spectroscopic techniques. Furthermore, the electrochemical properties of the material have been investigated using galvanostatic cycling, cyclic voltammetry (CV), and electrochemical impedance spectroscopy (EIS), and structural/morphological changes that occurred both on the cathode and anode side during cycling were probed by ex situ XRD, XPS, field-emission scanning electron microscopy (FESEM), and Raman spectroscopy.

2. Results and Discussion

The structure of $WOCl_4$ was analyzed by Rietveld refinement[12] of X-ray powder diffraction data using the GSAS program.[13] **Figure 1**a shows the Rietveld-refined diffraction pattern of the pristine $WOCl_4$. Braggs peaks indicate that $WOCl_4$ crystallizes in the $I4$ space group with a tetragonal structure at room temperature (ICSD collection code 25 519). The unit cell parameters are $a = 8.4795$ Å, $b = 8.4786$ Å, $c = 3.9940$ Å, and $V = 287.10$ Å^3. The crystal structure is shown in the inset of Figure 1a, mainly consisting of the distorted octahedra of WO_2Cl_4, where two O (in red) lie opposite of the square plane formed by four Cl (green) atoms and a central W (purple). These octahedra are connected by oxygen bridges and form linear chains along the c-axis.

Alternating W—O bonds are asymmetric in length (3.2 Å) and followed by a bridging W—O bond with a length of 1.8 Å, while the Cl—O bond length was 2.83 Å.[14] The distorted octahedra result from the different sizes of Cl^- and O^{2-} ions as well as the polarization effect of W^{+6} ions. The X-ray diffraction (XRD) pattern of the $WOCl_4/C$ composite is shown in Figure S1, Supporting Information, which has slight peak broadening, indicative of particle size reduction due to ball milling. The FESEM images of the as-received $WOCl_4$ show elongated rod-shaped particles with lengths ranging from 100 to 1000 μm and width between 5 and 50 μm (Figure 1b). The ball-milled $WOCl_4/C$ samples show the formation of the uniform composite of $WOCl_4$ and carbon, with significant reduction in the size of $WOCl_4$ particles down to ≈10 μm. The electrochemical behavior of $WOCl_4$ as an active material in the positive electrode of CIB was studied in half cells with metallic lithium anode and 3 M $Pyr_{14}Cl$ in PC:EC (1:1) as electrolyte. As pristine $WOCl_4$ is electronically semiconducting in nature, the ball-milled electrode composite provides electronic conductivity within the carbon matrix. To overcome the issue of chloride-ion corrosion of stainless steel above 2.5 V,[15] Mo foil current collectors were used at the cathode side. The open-circuit potential (OCV) of the half cell was ≈3.9 V and to understand the window of the redox reactions involved, initially, CV was performed (**Figure 2**a). The first cathodic sweep included a distinct reduction peak in the region of 2.0–0.5 V. In reverse sweep, the first oxidation peak was observed at 3.0–3.9 V. The peak positions shifted, and

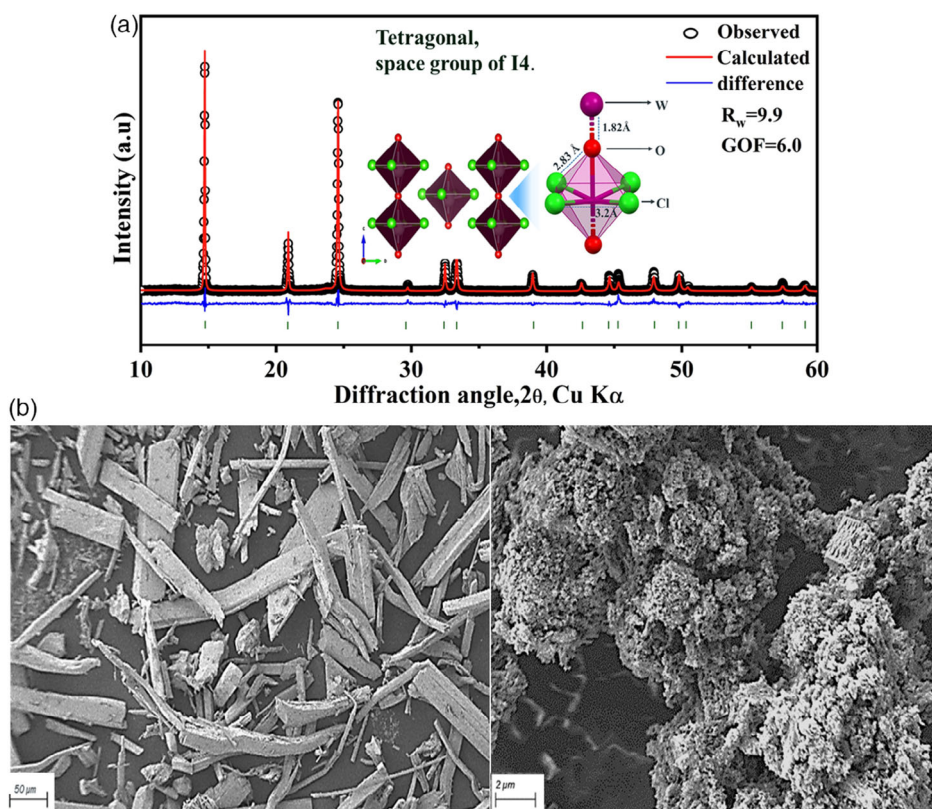**Figure 1.** a) Rietveld-refined XRD pattern of $WOCl_4$. Insets: structure of the tetragonal phase and schematic of WO_2Cl_4 octahedra (W purple, O red, Cl green). b) FESEM images of pristine $WOCl_4$ (left) and ball-milled $WOCl_4$/carbon composite (right).
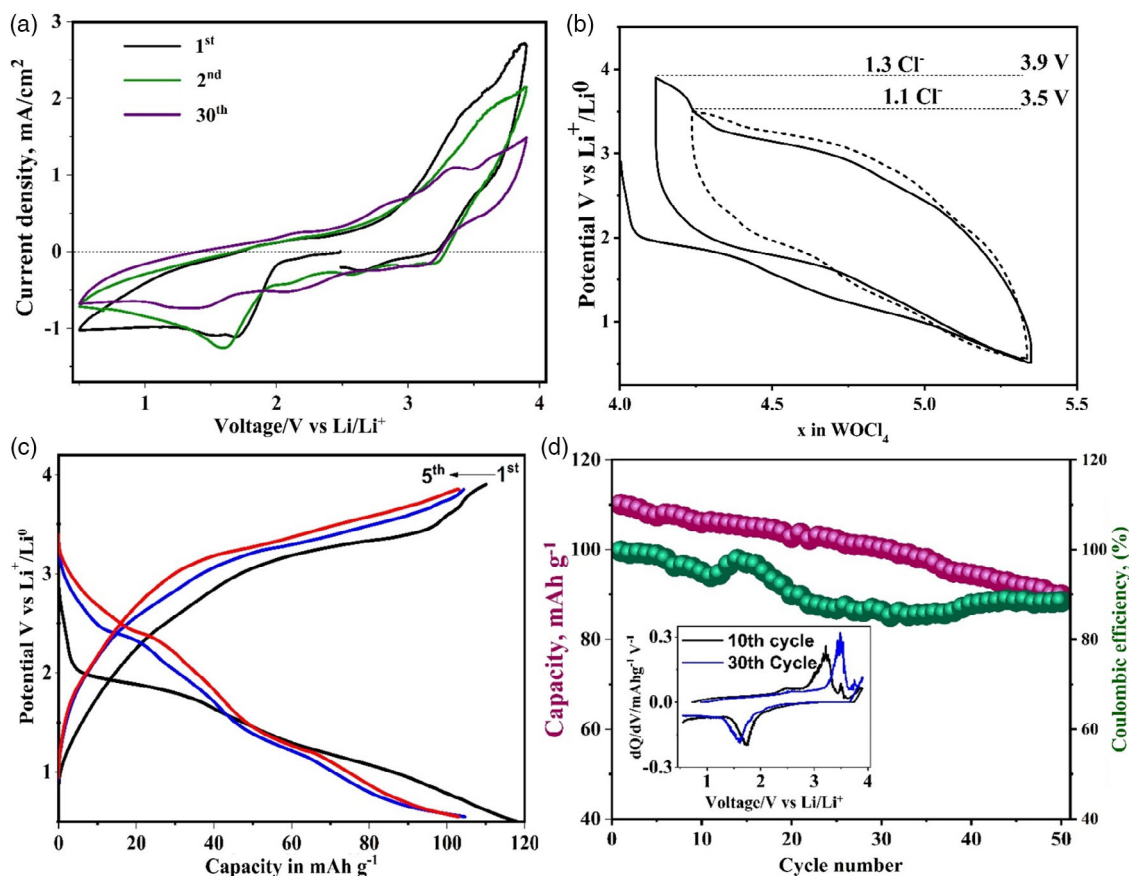
Figure 2. Electrochemical performance of WOCl$_4$ electrodes: a) Cyclic voltammogram profiles of WOCl$_4$ electrode after first, second, and 30th cycles. b) Voltage composition profile. c) Galvanostatic discharge–charge profile. d) Cycling performance of WOCl$_4$ at 0.5–3.9 V at C/10 rate; inset: differential capacity, dQ/dV plots of selected cycles at C/10 rate. Anode: Li metal, cathode: WOCl$_4$, electrolyte: 3 M Pyr$_{14}$Cl in PC:EC (1:1), separator: Glass fiber membrane.

intensities gradually decreased in the later cycles. This hints at an irreversible phase loss, in the initial cycles and formation of secondary/ or mixture of phases.

Figure 2b shows the voltage versus composition profile of WOCl$_4$ electrode, during electrochemical cycling, in the voltage range of 0.5–3.9 V at a current density of 100 mA g^{-1}. During first discharge, a sloping voltage profile with a plateau-like behavior around 1.7 V could be observed. The first discharge capacity was 120 mAh g^{-1} (38% of theoretical capacity of 313 mAh g^{-1}) and corresponds to a removal of ≈1.35 Cl$^-$ ions per formula unit (f.u.) based on electron counting. In the consecutive charge, 1.1 and 1.3 Cl$^-$ ions per f.u. could be inserted back for 3.5 and 3.9 V versus Li/Li$^+$, respectively. This corresponds to an overall reversible capacity of 100 mAh g^{-1}, as shown in Figure 2c. The second cycle showed a similarly sloping voltage profile, but with a slight shift of the voltage plateau to a higher voltage (≈2.5 V), which can be associated with structural changes during the first cycle. WOCl$_4$ exhibited a capacity retention of 90 mAh g^{-1} (coulombic efficiency: ≈90%) after 50 cycles, as shown in Figure 2d. The difference in the initial and latter voltage profiles, as can be observed by CV and differential capacity plots (inset in Figure 2d), indicates a chloride-ion shuttle that involves change in structural coordination, which we will investigate by different

ex situ measurements, such as XRD, Raman spectroscopy, and XPS in more detail.

Figure 3a shows the X-ray diffractograms collected on the cathodes retrieved from Li/3 M Pyr$_{14}$Cl in PC:EC (1:1)/WOCl$_4$ electrochemical cell, at different states of cycling. Upon first discharge, a strong loss in crystallinity results in the appearance of a new broad reflection centered at 2θ value of 11.6, indicative for the formation of an amorphous phase. The transformation of crystalline phase to an amorphous phase suggests an irreversible structural modification likely associated with a conversion-type mechanism.[16] Amorphization is a common observation in conversion-based electrodes and it is challenging, to characterize such materials. For example, the amorphization phenomenon has been reported from Mössbauer spectroscopy studies of the lithiation process in Fe$_{0.5}$TiOPO$_4$[17] and SnO$_2$[18] electrodes. The chloride-ion cathodes such as BiOCl[3g,19] and FeOCl have witnessed similar behavior. This was attributed to the formation of amorphous and/or nanosized particles.[11] During dechlorination, the chloride-deficient WOCl$_{4-x}$ phase leads to phase separation and/or amorphization of the electrode material. Thus, it was difficult to identify the exact phase after discharge, due to loss of crystallinity of the electrode. The diffraction pattern of the charged sample shows similar amorphous pattern. To get
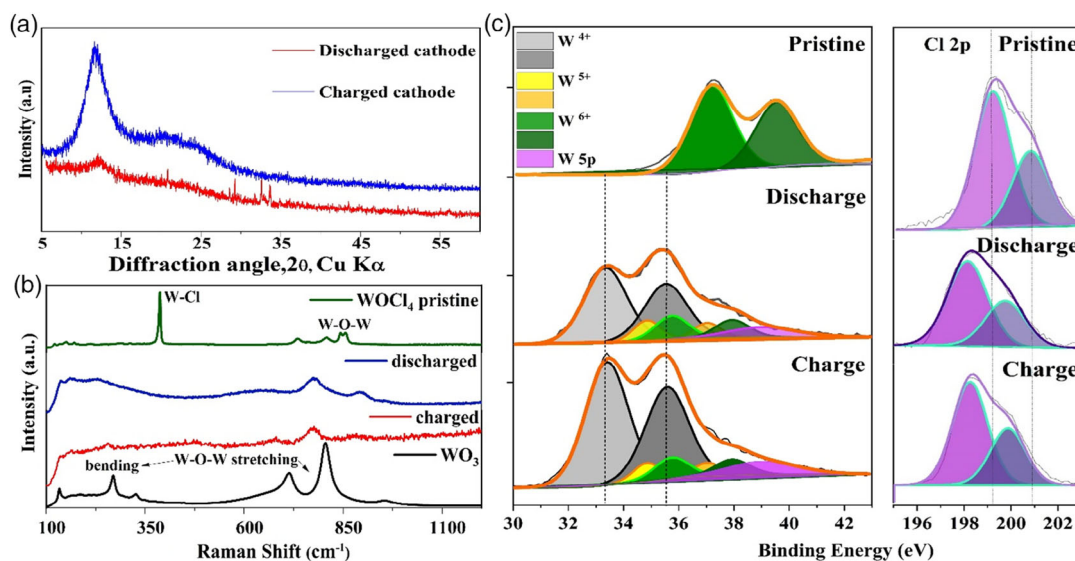
ADVANCED
SCIENCE NEWS
www.advancedsciencenews.com

Energy Technology
Generation, Conversion, Storage, Distribution
www.entechnol.de

Figure 3. Ex situ characterization of WOCl$_4$ after electrochemical cycling: a) X-ray diffractograms of WOCl$_4$ after first discharge and charge. b) Comparative Raman spectra of WOCl$_4$ after discharge, charge and c) W 4f and Cl 2p XPS spectra of pristine, discharged, and charged electrode.

further information on discharged products, complementary characterization techniques are necessary, which will be discussed in later sections. Figure S2, Supporting Information, shows the X-ray diffractogram of the anode (lithium metal) after discharge, which clarifies the formation of LiCl. This confirms the chloride-ion shuttle in the cell from cathode to anode during cycling.

The FESEM analysis of discharged and charged cathodes is shown in Figure S3, Supporting Information. Both samples show bulkier particles with modified surfaces. It reveals electrically disconnected bulkier cathode particles from conductive carbon, which possibly results from volume expansion during electrochemical cycling. The energy-dispersive X-ray (EDX) elemental mapping of these electrodes indicates the presence of W, O, and Cl in electrodes. The reduction of chloride content during discharge, and increase in the same upon charging, indicates reversible chlorination/dechlorination.

Raman spectroscopy measurements of the pristine WOCl$_4$ sample (Figure 3b) showed three active Raman active modes, A, B, and E.[14] The double band occurring at 877 and 888 cm^{-1} represents the stretching of the W–O–W linear chain, while the main band at 400 cm^{-1} corresponds to W–Cl stretching. Raman spectra of the discharged electrode display new vibrational modes, while the W–Cl stretching band of WOCl$_4$ disappears. The weaker bands at 139 and 162 cm^{-1} correspond to W–Cl stretching, at 264 cm^{-1} correspond to O–W–Cl,[20] while the features at 704, 807, and 930 cm^{-1} are assigned to lattice bending (δ) vibrations of W–O–W, stretching (ν) of W–O, and W–O–W respectively. These new vibrational modes indicate the formation of a WO$_3$-like structure. Finally, the small shift of the W–O bending mode from 710 to 698 cm^{-1} could be due to an increase in bond length,[21] associated with the change in the oxidation state or ionic coordination within the structure.

XPS analysis was carried out on a pristine WOCl$_4$ sample, an electrode discharged to 0.5 V, and an electrode charged to 3.9 V. Figure 3c shows the intensity-normalized detail spectra in the W 4f and Cl 2p region. The W 4f spectra of the pristine sample show a W 4f peak doublet at 36.6 and 38.8 eV, which can be assigned to W (+VI) in WOCl$_4$.[22] Correspondingly, the peak doublet in the Cl 2p spectrum at 199.2 and 200.8 eV is due to chloride in WOCl$_4$.[22] For the discharged and charged samples, the features of WOCl$_4$ disappear. Instead, three new peak doublets are observed in the W 4f spectra of these two samples. The first doublet at 35.8 and 37.0 eV is most probably due to W^{6+} but in a different chemical surrounding and binding energy (BE) value corresponds to that of WO$_3$,[22,23] while the second doublet at 34.8 and 36.0 eV is probably related to W^{5+} species.[24] The third doublet at 33.4 and 34.6 eV is due to W^{4+}.[25] The observed peak positions of the second and third feature are slightly above the expectation for pure oxide compounds of this oxidation state and it can be speculated that this slight shift of the BE could originate from some Cl$^-$ coordination process in the lattice. Tungsten oxychlorides with W oxidation states lower than +III (i.e., WOCl$_4^{3-}$) are unstable in chloride ion-rich electrolytes and tend to be converted to tungsten chlorides.[26] The observation of a lower oxidation state of tungsten can be ascribed to the partial reduction of W^{6+} into W^{5+} and W^{4+}, in compliance with the dissociation of Cl$^-$ ions from WOCl$_4$ during the discharge process. Furthermore, it is known that metal chlorides such as W(+VI)Cl$_6$ are known to get reduced into tungsten(+V) in chloride-rich electrolytes/melts, which is attributed to the oxidation of the chloride ion by tungsten (+VI) or due to reaction with Cl$^-$.[27] The spectra in the Cl 2p range shows for both cycled samples a single peak doublet at 198.2 and 199.8 eV due to some metal chloride but not metal oxychloride. These results corroborate again the pronounced changes in the chemical environment from M–O–Cl, likely to separate M–O and M–Cl.[28] XPS is also performed on the cathode side, as shown in Figure S4, Supporting Information. The absence of peak at a BE value of ≈55.0 eV indicates that there is no lithium ion crossover from the anode side.

ADVANCED
SCIENCE NEWS

www.advancedsciencenews.com

Energy Technology
Generation, Conversion, Storage, Distribution

www.entechnol.de

In view of the Raman and XPS results, it can be concluded that WO_3-type species are formed irreversibly during the discharge process without complete reconversion upon charging, while XPS explicitly shows varying amounts of metal-coordinated chloride, which could be tungsten with +6 and/or its reduced states. Thus, WO_3 and WCl_x ($x = 4,5,6$) are the probable discharge products. After first discharge, tungsten chloride participates electrochemically to shuttle chloride ions to the anode. An impedance analysis of the cells in the OCV condition, discharged, and charged state is shown in Figure S5, Supporting Information. It is evident that impedance increases after the first discharge by one order of magnitude and does not reduce after the charge. The capacity fading over the number of cycles could be linked to volume changes resulting from metal-to-metal chloride conversion, which in the case of WCl_4–WCl_6 is 59.8%.[7] Generally, the large volume changes during discharge/charge processes induce not only drastic pulverization, consequent loss of electrical contact between active materials/the collector, but also formation of the solid–electrolyte interphase (SEI) layer on the conversion-induced electrode/electrolyte interface, which generally leads to low coulombic efficiency and rapid capacity fading.[18a] In addition, the discharge product on anode, LiCl, is electronically insulating in nature and would also contribute to the total resistance of the cell.[29] On the other hand, we cannot rule out the possibility of partial dissolution of cathode material in the liquid electrolyte, which could cause capacity fading. However, comprehensive advanced characterization methods are necessary, to understand the detailed mechanism.

3. Conclusion

In summary, we have investigated tungsten oxychloride as a novel candidate positive electrode material for CIBs, using non-aqueous 3 M $Pyr_{14}Cl$ in PC: EC (1:1) electrolyte and lithium metal as anode. The cathode shows a first discharge capacity of 120 mAh g^{-1} and a reversible capacity of 90 mAh g^{-1} after 50 cycles at a rate of C/10. Ex situ characterization comprising XRD, XPS, Raman spectroscopy, and FESEM revealed that the storage mechanism is based on a conversion reaction, with chloride ions shuttling from negative to positive electrode back and forth. The strong capacity fading is likely to be associated with the large volume changes due to the conversion reaction. Further studies on engineering the cathode material to overcome the volume changes and possible dissolution in electrolyte would be beneficial in achieving the improved performance. Considering its promise as a cathode, this work paves a way forward to use tungsten chloride-based materials in battery applications.

4. Experimental Section

Synthesis of Cathode/Conductive Carbon Composite: The commercial $WOCl_4$ powder was purchased from Sigma Aldrich. A cathode composite of $WOCl_4$ and conductive carbon (Super P, Alfa Aesar) was formed by mechanical milling in the ratio of 80:20 ($WOCl_4$:C) at 400 rpm for 1 h. Milling was carried out in a planetary ball mill (Fritsch PULVERISETTE 6) with an 80 mL silicon nitride vial and silicon nitride balls. The ball-to-powder ratio was 20:1. All steps were carried out in inert gas atmosphere.

Preparation of the Electrolyte: Prior to electrolyte preparation, the chloride ion-conducting salt 1-Butyl-1-methylpyrrolidinium chloride ($Pyr_{14}Cl$, 99%, purchased from Iolitec) dried in a vacuum oven at 120 °C. The solvents propylene carbonate (PC) and ethylene carbonate (EC) were dried using molecular sieves (3 Å, Fisher chemical). The electrolyte was prepared by dissolving 3 M $Pyr_{14}Cl$ in PC:EC with a weight ratio of 1:1 in an inert atmosphere.

Characterization: XRD measurements were conducted in a Stadi P diffractometer (STOE & Cie) with a MYTHEN detector using a Cu Kα X-ray source with a wavelength of 1.5418 Å. The morphology of the samples was studied using FESEM (Carl-Zeiss LEO 1530 instrument). The chemical state of the elements was determined by XPS measurements using monochromatized Al Kα (1486.6 eV) radiation (Specs XPS system with a Phoibos 150 energy analyzer). The samples were kept under Ar, during transfer, to the XPS system. For BE calibration, the C 1s main peak was set to 284.8 eV. Peak fitting was done with Casa XPS using Shirley-type backgrounds and Gaussian–Lorentzian peak profiles. Raman spectroscopical measurements were performed in a confocal Raman microscope (InVia, RENISHAW), at room temperature ($\approx$25 °C) in the spectral range 100–1200 cm^{-1} using a HeNe laser with a wavelength of 532 nm as the excitation source. A 50× objective (Carl Zeiss) was used to focus the laser light onto the electrode surface and to collect the Raman signal. The laser power was $\approx$1.0 mW. The spectrum acquisition time was 1 s.

Electrochemical Tests: The electrochemical tests were carried out in a multichannel electrochemical workstation (VMP-3, Bio-Logic). The galvanostatic charge–discharge cycling and CV of the half cells were performed in the voltage range of 0.5–3.9 V and a current density of 100 mA g^{-1} at room temperature. EIS was performed with an applied sinusoidal excitation voltage of 10 mV in the frequency range from 1 MHz to 0.01 Hz. The loading of the active material was around 2 mg cm^{-2}. Lithium metal was used as an anode. Glass fiber membranes (Whatman) were used as the separator between the two electrodes. The two electrode Swagelok-type cells were fabricated in an argon-circulated glove box, with oxygen and moisture levels below 0.1 ppm.

Supporting Information

Supporting Information is available from the Wiley Online Library or from the author.

Conflict of Interest

The authors declare no conflict of interest.

Data Availability Statement

The data that support the findings of this study are available from the corresponding author upon reasonable request.

[1] a) T. C. Wanger, *Conserv. Lett.* **2011**, *4*, 202; b) A. Ajanovic, R. Haas, *Fuel Cells* **2019**, *19*, 515; c) T. Kim, W. Song, D.-Y. Son, L. K. Ono, Y. Qi, *J. Mater. Chem. A* **2019**, *7*, 2942.

[2] a) G. Karkera, A. S. Prakash, *ACS Appl. Mater. Interface* **2019**, *11*, 27870; b) S. G. Chandrappa, P. Moni, G. Karkera, A. S. Prakash, *Nanoscale Adv.* **2019**, *1*, 2392.

[3] a) Z. Li, O. Fuhr, M. Fichtner, Z. Zhao-Karger, *Energy Environ. Sci.* **2019**, *12*, 3496; b) E. Edison, S. Sreejith, C. T. Lim, S. Madhavi, *Sustainable Energy Fuels* **2018**, *2*, 2567; c) J. Bodart, N. Eshraghi, T. Carabin, B. Vertruyen, R. Cloots, F. Boschini, A. Mahmoud, *J. Power Sources* **2020**, *480*, 229057; d) D. Lu, H. Liu, T. Huang, Z. Xu, L. Ma, P. Yang, P. Qiang, F. Zhang, D. Wu, *J. Mater. Chem. A* **2018**, *6*, 17297; e) M. Sathiya, K. Ramesha, G. Rousse, D. Foix, D. Gonbeau, K. Guruprakash, A. S. Prakash, M. L. Doublet, J. M. Tarascon, *Chem. Commun.* **2013**, *49*, 11376; f) J. Ming, J. Guo, C. Xia, W. Wang, H. N. Alshareef, *Mater. Sci. Eng. R: Rep.* **2019**, *135*, 58; g) X. Zhao, Z. Zhao-Karger, D. Wang, M. Fichtner, *Angew. Chem. Int. Ed.* **2013**, *52*, 13621; h) J. Luo, Q. Yin, J. Zhang, S. Zhang, L. Zheng, J. Han, *ACS Appl. Energy Mater.* **2020**, *3*, 4559; i) M. Anji Reddy, M. Fichtner, *J. Mater. Chem.* **2011**, *21*, 17059.

[4] G. Karkera, M. A. Reddy, M. Fichtner, *J. Power Sources* **2021**, *481*, 228877.

[5] a) P. Gao, M. A. Reddy, X. Mu, T. Diemant, L. Zhang, Z. Zhao-Karger, V. S. K. Chakravadhanula, O. Clemens, R. J. Behm, M. Fichtner, *Angew. Chem. Int. Ed.* **2016**, *55*, 4285; b) L. Chen, H. Yu, W. Li, M. Dirican, Y. Liu, X. Zhang, *J. Mater. Chem. A* **2020**, *8*, 10709; c) D. Bosubabu, R. Sampathkumar, G. Karkera, K. Ramesha, *Energy Fuels* **2021**, *35*, 8286; d) S. A. Pervez, B. P. Vinayan, M. A. Cambaz, G. Melinte, T. Diemant, T. Braun, G. Karkera, R. J. Behm, M. Fichtner, *J. Mater. Chem. A* **2020**, *8*, 16451.

[6] Z. D. Sharp, D. S. Draper, *Earth Planet. Sci. Lett.* **2013**, *369–370*, 71.

[7] X. Zhao, S. Ren, M. Bruns, M. Fichtner, *J. Power Sources* **2014**, *245*, 706.

[8] Q. Yin, J. Luo, J. Zhang, S. Zhang, J. Han, Y. Lin, J. Zhou, L. Zheng, M. Wei, *Adv. Funct. Mater. 30*, 1907448.

[9] H. Li, M. Li, H. Zhao, T. Li, Z. Fang, *J. Power Sources* **2021**, *512*, 230507.

[10] T. Xia, Y. Li, L. Huang, W. Ji, M. Yang, X. Zhao, *ACS Appl. Mater. Interface* **2020**, *12*, 18634.

[11] X. Zhao, Q. Li, T. Yu, M. Yang, K. Fink, X. Shen, *Sci. Rep.* **2016**, *6*, 19448.

[12] L. B. McCusker, R. B. Von Dreele, D. E. Cox, D. Louer, P. Scardi, *J. Appl. Crystallogr.* **1999**, *32*, 36.

[13] B. H. Toby, *Powder Diffr.* **2006**, *21*, 67.

[14] J. Gabrusenoks, *IOP Conf. Ser.: Mater. Sci. Eng.* **2015**, *77*, 012032.

[15] J. Muldoon, C. B. Bucur, A. G. Oliver, J. Zajicek, G. D. Allred, W. C. Boggess, *Energy Environ. Sci.* **2013**, *6*, 482.

[16] P. Bleith, M. Valla, P. Novák, C. Villevieille, *J. Mater. Chem. A* **2014**, *2*, 12513.

[17] P. Bleith, H. Kaiser, P. Novák, C. Villevieille, *Electrochim. Acta* **2015**, *176*, 18.

[18] a) Z. Huang, H. Gao, Z. Yang, W. Jiang, Q. Wang, S. Wang, J. Ju, Y.-U. Kwon, Y. Zhao, *Mater. Des.* **2019**, *180*, 107973; b) E. Umeshbabu, M. Satyanarayana, G. Karkera, A. Pullamsetty, P. Justin, *Mater. Adv.* **2022**, *3*, 1642.

[19] P. Gao, X. Zhao, Z. Zhao-Karger, T. Diemant, R. J. Behm, M. Fichtner, *ACS Appl. Mater. Inter.* **2014**, *6*, 22430.

[20] R. Mattes, F. Schröder, *Z. Naturforsch.* **1969**, *24b*, 1095.

[21] F. Wan, H. Shi, W. Chen, Z. Gu, L. Du, P. Wang, J. Wang, Y. Huang, *Nanomater* **2017**, *7*, 210.

[22] A. I. Smith, H. V. Wladkowski, Z. H. Hecht, Y. She, S. Kattel, P. I. Samarawickrama, S. R. Rich, J. R. Murphy, J. Tian, J. F. Ackerman, W. D. Rice, E. B. Hulley, B. M. Leonard, *Chem. Mater.* **2020**, *32*, 10482.

[23] C. B. Rodella, D. H. Barrett, S. F. Moya, S. J. A. Figueroa, M. T. B. Pimenta, A. A. S. Curvelo, V. Teixeira da Silva, *RSC Adv* **2015**, *5*, 23874.

[24] F. Y. Xie, L. Gong, X. Liu, Y. T. Tao, W. H. Zhang, S. H. Chen, H. Meng, J. Chen, *J. Electron. Spectrosc. Relat. Phenom.* **2012**, *185*, 112.

[25] P. Chen, M. Baldwin, P. R. Bandaru, *J. Mater. Chem. A* **2017**, *5*, 14898.

[26] I. W. Sun, A. G. Edwards, G. Mamantov, *J. Electrochem. Soc.* **1993**, *140*, 2733.

[27] a) T. B. Scheffler, C. L. Hussey, *Inorg. Chem.* **1984**, *23*, 1926; b) G. Carountzos, C. G. Kontoyannis, T. Østvold, *Ber. Bunsen. Phys. Chem.* **1997**, *101*, 847.

[28] R. P. Vasquez, *Surf. Sci. Spectra* **1993**, *2*, 138.

[29] X. Liang, Q. Pang, I. R. Kochetkov, M. S. Sempere, H. Huang, X. Sun, L. F. Nazar, *Nat. Energy* **2017**, *2*, 17119.